Dynamics of linear and T-shaped Ar–I_2 dissociation upon $B \leftarrow X$ optical excitation: A dispersed fluorescence study of the linear isomer

Amy E. Stevens Miller, Cheng-Chi Chuang, Henry C. Fu, Kelly J. Higgins, and William Klemperer
Department of Chemistry and Chemical Biology, Harvard University, Cambridge, Massachusetts 02138

(Received 3 June 1999; accepted 11 August 1999)

We report the dispersed fluorescence spectra of the linear and the previously well-studied T-shaped isomers of Ar–I_2 following $B \leftarrow X$ optical excitation for $v_{\text{pump}} = 16-26$, below the I_2 dissociation limit. The linear isomer has a continuum excitation spectrum. For excitation at the highest pumping energy ($v_{\text{pump}} = 26$), the product vibrational state distribution is nearly identical to that observed for excitation above the $I_2(B)$ dissociation limit; it shows a broad, nearly Gaussian distribution of $I_2(B)$ vibrational states, with about 22% of the available excess energy deposited in translation of the Ar+I_2. This gives direct evidence that the ''one-atom cage'' effect seen above the $I_2(B)$ dissociation limit is attributable to the linear Ar–I_2 isomer. The product vibrational state distribution becomes increasingly Poisson for decreasing excitation energies, and only about 7% of the excess energy is deposited in translation for $v_{\text{pump}} = 16$. The bond energy in the linear isomer is determined from the spectra, $170(\pm 1.5) \leqslant D_0''(\text{linear Ar–I}_2(X)) \leqslant 174(\pm 1.5)\ \text{cm}^{-1}$. A bond energy of $D_0''(\text{T-shaped Ar–I}_2(X)) = 142 \pm 15\ \text{cm}^{-1}$ is estimated based on the linear to T-shaped population ratio observed in the beam, which is about 90 cm^{-1} smaller than that determined from fluorescence spectra. We suggest that electronic quenching in the T-shaped isomer is nearly 100% for the highest vibrational level produced by vibrational predissociation. © *1999 American Institute of Physics.* [S0021-9606(99)02041-3]

I. INTRODUCTION

The binding, structure, and dynamics of van der Waals complexes of rare gases with halogens have been the subjects of long-standing investigation.[1] Studies on Ar–I_2 have been most prominent,[2–5] due to the readily accessible optical spectrum of I_2 together with the facile, inexpensive production of Ar–I_2. In pioneering research, Blazy, DeKoven, Russell, and Levy established the existence of the T-shaped isomer of Ar–I_2; they observed vibrationally-resolved fluorescence emanating from B state I_2 following the $B \leftarrow X$ electronic excitation of Ar–I_2.[3]

The 1981 report by Saenger, McClelland, and Herschbach[6] showed that fluorescence of free I_2 could be observed following excitation of Ar–I_2 up to 1400 cm^{-1} above the dissociation limit of I_2. This result was soon confirmed by Valentini and Cross,[7] who observed the dispersed fluorescence of the free I_2 after excitation of ArI_2 by 488 nm radiation. They suggested that the ''one-atom caging'' effect is the result of impulsive transfer of the iodine atom vibrational energy to translational energy of the argon atom. This energy transfer was also seen by Philippoz, van den Bergh, and Monot,[8] who reported the vibrational state distributions of I_2 from fluorescence observed following excitation of the I_2 $B \leftarrow X$ transition above the B-state dissociation limit in the complexes Ar–I_2, Ne–I_2, and Kr–I_2. For all cases, the vibrational distributions show broad gaussian distributions, with an average vibrational energy loss for the Ar–I_2 of about 22% of the total excess energy deposited in B state Ar–I_2. Various dynamical calculations used to model the energy transfer based on the presumed T-shaped geometry gave results in poor agreement with the observed amount of I_2 to Ar energy transfer.[9–11] Such impulsive energy transfer could readily be the result of a linear isomer of Ar–I_2. However, this isomer was not believed to be present in the adiabatic expansion, since the very low effective temperature generally produces considerable selectivity and it was generally assumed that only one isomer is present with enough population to be detected. In a little noted paper, Brown, Schwenke, and Truhlar reported the calculated potential energy surface of He–I_2; they found comparable minima for linear and T-shaped geometries.[12]

Fluorescence studies of Ar–I_2 were continued by Burke and Klemperer;[5] they collected total fluorescence following excitation of the Ar–I_2 ($B \leftarrow X$) band. They were able to partially rotationally-resolve the excitation spectrum, thereby determining the rotational constants of the T-shaped Ar–I_2 in the X and B states. More importantly, in addition to the absorption band of the T-shaped isomer, they observed a wavelength-independent fluorescence, which they attributed to the fluorescence from continuum excitation onto a repulsive potential surface of the linear isomer of Ar–I_2. Their data gave the first indication that both linear and T-shaped isomers are present under the identical expansion conditions. Additional experimental indications of the existence of two geometrically distinct isomeric forms has been given by the photoionization studies of Cockett, Beattie, Donovan, and Lawley.[13] Since these works, the dynamics of the Ar–I_2 photodissociation has been re-examined using a linear Ar–I_2 geometry,[11,14,15] and other calculations have shown the coexistence of linear and T-shaped Ar–I_2 complexes in the elec-

tronic ground state.[16–18] For example, recent theoretical work by Kunz, Burghardt, and Hess,[18] using a supermolecular *ab initio* calculation, has shown the coexistence of linear and T-shaped Ar–I_2, with calculated well depths (D_e) of 192.5 cm^{-1} and 179.2 cm^{-1}, respectively. Most recently, Burroughs, Van Marter, and Heaven[19] have reported that fluorescence-depletion, i.e., ''hole-burning,'' experiments demonstrate that fluorescence from free I_2 produced from excitation above the *B*-state dissociation limit is not depleted with excitation into the T-shaped $B \leftarrow X$ band of Ar–I_2; they did observe fluorescence depletion from the adjacent continuum which had been assigned to the linear isomer by Burke.[5]

Linear isomers of rare-gas halogen complexes have been confirmed by direct observation of the rotational spectroscopy of Ar–ClF (Ref. 20) and He–ClF.[21] For He–ClF, not only were pure rotational transitions of both the linear and the T-shaped isomer observed, but direct transitions between the linear and the T-shaped isomers establish the linear isomer to be the lower in energy. The experimental data and calculated potential curves indicate both the linear and T-shaped geometries are on the same, ground state potential energy surface of He–ClF.

Independent confirmation of the isomeric forms of Ar–I_2 is made difficult by the extremely small dipole moment of Rg–X_2, such that high resolution microwave spectroscopy on Rg–I_2 is difficult. In an elegant microwave study, Xu, Jäger, Ozier, and Gerry observed only the T-shaped isomer of $ArCl_2$.[22] Studies on Rg–X_2 systems have been mainly conducted via the $B \leftarrow X$ electronic excitation of X_2, for example, Ne–Br_2,[23] Ne–Cl_2,[24] and Ar–Cl_2,[25] and only T-shaped structures have been found.

In this paper, we extend the work of Burke[5] by dispersing the laser-induced fluorescence of linear Ar–I_2 in the spectral region of 571 nm ($v=16$) to 543 nm ($v=26$), to obtain the nascent vibrational populations of $I_2(B)$ produced by dissociation of Ar–I_2 following excitation of the $B \leftarrow X$ transition in the complex. As indicated by Burke,[5] the $B \rightarrow X$ fluorescence from excitation of linear Ar–I_2, when integrated over all excitation wavelengths, is 2.1 ± 0.4 times the total integrated fluorescence of the T-shaped isomer. However, the measured fluorescence of the linear isomer at any particular wavelength is approximately 15 times weaker than the peak fluorescence intensity of the T-shaped isomer, as the excitation is split into a continuum. In view of the impossibility of saturating an absorption continuum, the present work exploits the intracavity excitation technique to obtain the relatively weaker dispersed LIF signal for the linear isomer of Ar–I_2. Our methodology and results are strikingly similar to the work of Philippoz *et al.*,[8] where fluorescence was dispersed following excitation above the *B* state dissociation limit.

II. EXPERIMENT

The Ar–I_2 was formed in a molecular beam apparatus which was designed to fit within the cavity of a cw ring dye laser (Coherent model 899-21); the apparatus is shown schematically in Fig. 1. The molecular beam chamber consists of a 4 in. o.d. ''tee'' which is mounted inverted and with the tee

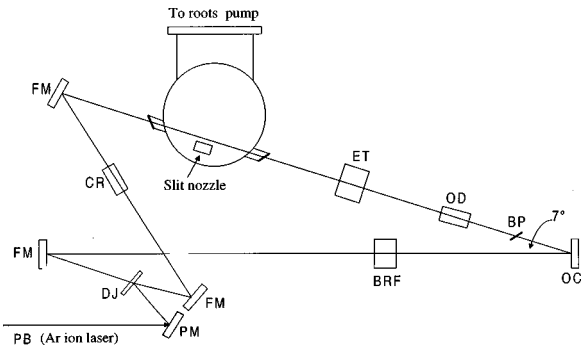

FIG. 1. Schematic diagram of the vacuum chamber and ring dye laser cavity (Coherent 899-21) components. PB, pump beam (Ar ion laser beam); PM, pump mirror; FM, folding mirror; DJ, dye jet; CR, compensation rhomb; ET, thin and thick étalons; OD, optical diode; BRF, birefringent filter; BP, brewster plate; OC, output coupler (1%). The vacuum chamber is composed of a 4 in. o.d. T-tube and is positioned inside the laser cavity. The slit nozzle, oriented 7° with respect to the horizontal, is parallel to the ''intersecting'' laser beam.

perpendicular to the laser beam, in the region above the dye jet. The laser beam enters and exits the chamber through Brewster windows glued to 1/2 in. o.d. tubing mounted in Cajon-ultra-Torr fittings. The laser beam is at a 7° angle with respect to horizontal at the intersection with the chamber; the cajons are mounted at a similar angle, and ~0.5 in. below the tubing center line. The chamber, in combination with the Brewster windows settings, fits in the available space within the laser cavity. The chamber is pumped from above by a Roots-type mechanical blower with pumping speed 300 ℓ/s.

The argon used in the expansion flowed through a bubbler which was filled with I_2 and teflon chips (to increase the surface area) and held at 60 °C. The inlet line following the bubbler was held at 70 °C to prevent condensation of the I_2. The Ar–I_2 complex was formed by supersonic jet expansion through a slit nozzle (100 μm×8 mm), located 5–6 mm below the laser beam. The backing pressure behind the nozzle was 15–30 psi, resulting in a chamber pressure of 20–60 mTorr. The dye laser was pumped by 6–8 W of light from an argon-ion laser operating in a multiwavelength mode. Two different output couplers were used during these experiments; with a nominally 2% output coupler the dye laser output power was 300 mW, which corresponds to a circulating intracavity power of 15 W. Replacing the coupler with a 1% output coupler resulted in an intracavity power ~4 times higher, or 60 W (the output power was too low to measure directly). The frequency stabilization was 1 MHz for the long periods of integration time needed for acquisition of the data shown here. Fluorescence was collected by a single 2 in. diam $f/3$ lens located ~12 in. from the interaction region. The image was rotated from nearly horizontal to nearly vertical by two mirrors, and then reimaged at the entrance slit of a 0.5 m ($f/6.9$) monochromator (Acton Research Corporation SpectraPro-500). Since the entrance slit is vertical, the uniform section of the laser/molecular beam fluorescence image corresponds to sampling across a narrow, uniform region which is parallel to the slit nozzle, i.e., which corresponds to a region of uniform temperature and jet conditions. Moving the nozzle to laser distance made no changes in the observed

vibrational populations or spectral features. The monochromator was operated with a grating ruled at 300 grooves/mm, which provides adequate resolution of the vibrational bands. Fluorescence was detected with a silicon array detector (Princeton Instruments, RY-512), operating at $-20\,^{\circ}\mathrm{C}$. This experimental configuration gave coverage over 80 nm spectral range in a single data set. Spectra shown are spliced from several sets of overlapping data, obtained by changing the center wavelength of the grating by 50 nm. Each data set was accumulated over 10–30 min integration time.

With our experimental conditions (laser power levels, use of a slit jet, and appropriate heating of the I_2 in the inlet line), the fluorescence following excitation of uncomplexed I_2, T-shaped Ar–I_2, and linear Ar–I_2 in the jet was readily apparent and distinguishable by eye, considerably aiding the optimization of the system. The fluorescence from excitation of the T-shaped Ar–I_2 isomer is distinct from that from excitation of uncomplexed I_2 by the blue-shift in the excitation band; the fluorescence from excitation of the linear isomer is distinct by being noticeably lower intensity, and independent of laser wavelength.

III. RESULTS AND ANALYSIS

The lifetimes of the T-shaped Ar–$I_2(B)$ isomer is estimated to be 70 ps;[26] that for the linear isomer is estimated to be 150 fs, as discussed later in this paper. Since the lifetime of the complexes are orders of magnitude shorter than the radiative lifetime of the I_2 (10^{-6} s), the observed fluorescence signals originate from the dissociated $I_2(B)$ photofragment emission. The dispersed fluorescence spectra therefore reveal product vibrational state distributions of the $I_2(B)$ photofragment following dissociation of the complexes as has been shown in detail by Levy and co-workers.[3,4] Figures 2(a), 2(b), and 2(c) show the dispersed fluorescence spectra of I_2 monomer, T-shaped and linear Ar–I_2 isomers upon I_2 $B(v_{\mathrm{pump}}=24)\leftarrow X(v''=0)$ excitation. The locations of excitation frequencies for each isomer and validation for formation of binary Ar–I_2, rather than higher order $\mathrm{Ar}_m(I_2)_n$ ($m>1, n>1$), have been extensively discussed by Burke.[5] The T-shaped Ar–I_2 excitation band is discrete and is blue-shifted by 14 cm^{-1} with respect to the I_2 $B\leftarrow X$ band. The excitation spectrum for the corresponding linear isomer is broadly continuous. The dispersed fluorescence spectrum resulting from the continuous linear Ar–I_2 isomer feature, as in Fig. 2(c), is at a maximum when the pump laser frequency is tuned to within ± 5 cm^{-1} from the uncomplexed I_2 $B\leftarrow X$ band origin. The dispersed fluorescence from the continuous linear Ar–I_2 is approximately a factor of 2 lower in intensity in between the maxima. The relative fluorescence intensity distributions for both isomers show little variation as experimental conditions (i.e., backing pressure and I_2 concentration) are varied. This assures that the excitation is from the Ar–I_2 isomers, rather than higher order clusters, as well as that the I_2 product vibrational distribution is not irretrievably altered by collisions in the jet. The carrier gas density remains high using a slit, rather than pinhole jet, and some collisional relaxation of the nascent I_2 is unavoidable. The remarkable difference shown in the dispersed fluorescence spectrum between Fig. 2(b) and 2(c) demonstrates the coexistence of both linear and T-shaped Ar–I_2 isomers under identical conditions in the jet.

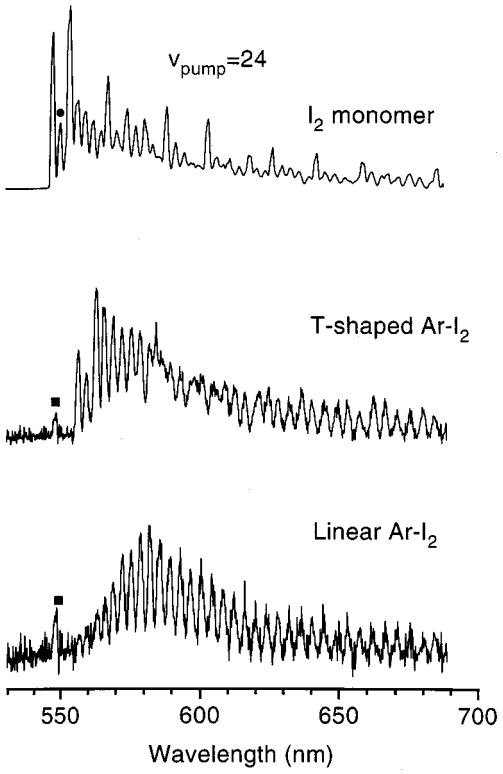

FIG. 2. Overview of dispersed fluorescence spectrum following $B(v_{\mathrm{pump}}=24)\leftarrow X(v''=0)$ excitation of (a) I_2 monomer (b) T-shaped Ar–I_2 and (c) linear Ar–I_2. The peaks indicated by ■ are due to laser scattering. A noticeable energy gap (three I_2 vibration quanta) between the pump laser and first fluorescence emission band [I_2 $B(v'=21)\rightarrow X(v'=0)$] in (b) clearly indicates that the product vibrational state distribution for the T-shaped complex is dominated by the $\Delta v=-3$ channel. For the linear Ar–I_2, the most intense feature in the dispersed fluorescence is peaked at 581.8 nm, or 33.6 nm red-shifted from the excitation wavelength. This peak has its main contribution from I_2 $B(v'=17)\rightarrow X(v''=2)$ emission. This indicates that for the linear isomer the dissociation process is quite facile, which leads to significant energy transfer from I–I vibration to fragments translation, with the most likely process loss of seven vibrational quanta from $I_2(B)$. The feature labeled by ● in (a) is due to the I_2 $(B,v'=23)\rightarrow X(v''=0)$ emission which is indicative of slight collisional relaxation in the jet.

To obtain details of the dissociation dynamics of the Ar–I_2 isomers in the B state, we have recorded the dispersed fluorescence spectra of both the T-shaped and the linear Ar–I_2 isomers following excitation in the spectral region of the I_2 $(B,v_{\mathrm{pump}}=16\text{–}26)\leftarrow(X,v''=0)$ transitions (corresponding to 571 nm to 543.5 nm in wavelength). To avoid the complexity from high order clusters of $\mathrm{Ar}_n(I_2)$, the spectra of the linear isomers were carefully recorded using an excitation within 1 cm^{-1} of the corresponding free I_2 $B\rightarrow X$ band origin. Determining the relative population of final product vibrational states from the measured dispersed fluorescence spectra is quite straightforward. The measured dispersed fluorescence intensity as a function of wavelength is determined by the relative population of final product vibrational states and the Franck–Condon factors (FCFs) of I_2 $B\leftarrow X$. We calculated the corresponding FCFs based on the well-determined I_2 X and B states RKR potentials[27] using

TABLE I. Product vibrational state distributions[a] of I_2 (B,v) following photodissociation of the linear Ar–I_2 complex upon I_2 B $(v_{pump}=26,24,22,20,18,16)\leftarrow X$ $(v''=0)$ excitation.

	Linear Ar–$I_2(B)$ v_{pump} state					
	26	24	22	20	18	16
v_{pump} (cm^{-1})[b]	18 402.7	18 240.2	18 070.1	17 892.2	17 708.5	17 516.5
I_2 product state						
23	3.9(0.3)	⋯	⋯	⋯	⋯	⋯
22	4.6(0.5)	⋯	⋯	⋯	⋯	⋯
21	8.3(0.8)	10.2(1.0)	⋯	⋯	⋯	⋯
20	9.0(0.9)	10.7(1.0)	14.0(1.4)	⋯	⋯	⋯
19	12.8(1.3)	12.2(1.2)	14.8(1.5)	⋯	⋯	⋯
18	**15.4**(1.5)	16.4(1.6)	18.8(1.9)	17.9(1.8)	⋯	⋯
17	12.6(1.3)	**17.5**(1.8)	**22.0**(2.2)	19.2(1.9)	⋯	⋯
16	11.6(1.2)	12.0(1.0)	11.4(1.1)	**23.2**(2.3)	**29.9**(3.0)	⋯
15	8.0(0.8)	11.3(1.1)	10.3(1.0)	16.1(1.6)	27.3(2.7)	⋯
14	7.2(0.7)	6.4(0.6)	6.0(0.6)	12.5(1.3)	17.8(1.8)	**44.6**(2.2)
13	3.5(0.4)	3.0(0.3)	2.7(0.3)	7.7(0.8)	15.0(1.5)	25.3(1.3)
12	2.8(0.3)	⋯	⋯	3.4(0.3)	9.9(1.0)	18.3(0.9)
11	⋯	⋯	⋯	⋯	5.7(0.6)	11.7(0.6)

[a]The product vibrational state distributions are extracted from the dispersed fluorescence spectra and corrected by taking collisional relaxation into account.
[b]The exact excitation laser frequency which is nearly equal to the corresponding I_2 $B\leftarrow X$ band origin.

LeRoy's LEVEL program.[28] The observed fluorescence intensity is also weighted by ν^{-3} to correct for spontaneous emission probability. Our fits were taken from the bluer emission; at redder wavelengths the grating efficiency decreases slightly and the fitted spectrum generally shows a higher intensity than that measured. The vibrational intervals of the B state have a spacing approximately half that of the X ground state. This results, at our level of resolution, in overlapping bands. In the spectra only the bluest emission features, $(v_h',0)$ and $(v_h'-1,0)$ are distinct. For lower vibrational levels, such as $v'=14$, the Franck–Condon factor for (14, 0) is almost an order of magnitude smaller than the redder features, (14, 1) and (14, 2). The redder features, however, consist of overlapping bands with transitions from smaller v'. For this reason we have only labeled the highest frequency feature, $(v_h',0)$ in the figures.

Under our experimental conditions, the $I_2(B)$ fragments produced from the photodissociation of Ar–I_2 undergo slight collisional relaxation prior to radiative decay to the ground electronic state. The measured product vibrational state distributions must be corrected for this relaxation. It is evident from the I_2 monomer dispersed fluorescence spectrum as shown in Fig. 2(a), that there is a significant amount of $I_2(B)$ at $v'=23$; the emission at 550.8 nm as denoted by ●, is the $I_2(B,v'=23)\rightarrow I_2(X,v''=0)$ transition. This shows that $I_2(B)$ at $v'=23$ is populated due to the collisional relaxation from the initially prepared $I_2(B,v'=24)$ state. The population ratio of $[I(v'=23)]/[I(v'=24)]$, with FCFs taken into account, is approximately 0.25. We recorded the I_2 monomer dispersed fluorescence from $v'=15$ to $v'=26$ and found that in our jet conditions the corresponding population ratio, $[I(v'-1)/I(v')]$, is invariant with the initially prepared v' state. This is also consistent with the results previously reported by Levy and co-workers.[3] The ratio of $\Delta v=-2/\Delta v=-1$ may be estimated to be near 1/4 from early collisonal relaxation measurements.[39] Thus the $\Delta v=-2$ collisional relaxation is too small to make a significant contribution to the fitted vibrational distribution, and therefore was assumed to be zero. We thus take the collisional relaxation into account and correct the product vibrational state distribution obtained from the measured dispersed fluorescence spectra. The results are summarized in Table I. Figure 3 represents the corrected product vibrational state distributions of linear Ar–I_2 upon I_2 $B(v_{pump})\leftarrow X(v''=0)$ excitation with v_{pump} ranging from 16 to 26.

There is no evidence of significant rotational excitation

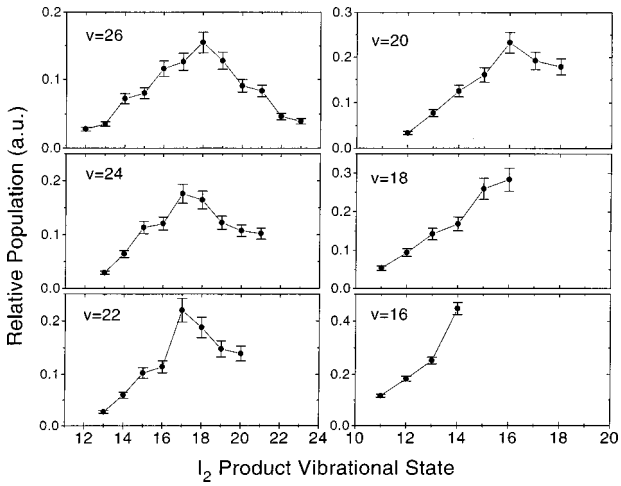

FIG. 3. The relative population of $I_2(B)$ product vibrational states resulting from photodissociation of linear Ar–I_2 following I_2 $B(v_{pump}=26,24,22,20,18,16)\leftarrow X(v''=0)$ excitation. The distribution for each v_{pump} state is deduced from the dispersed fluorescence spectra (as shown in Fig. 2(c)) incorporated with the corresponding I_2 $B\rightarrow X$ Franck–Condon factors. For consistency, the pump laser frequency used in each excitation is centered about the corresponding I_2 $B\leftarrow X$ band origin (less than ± 1 cm^{-1}). A gradual shift in the I_2 product vibrational distribution from Gaussian to Poisson is observed as v_{pump} varies from 26 $[r_{26}(\text{I–I})=3.35\,\text{Å}]$ to 16 $[r_{16}(\text{I–I})=3.19\,\text{Å}]$.

in the $I_2(B)$ produced from photodissociation of either the linear or T-shaped Ar–I_2. First, higher resolution spectra taken using a 1200 grooves/mm grating, but not shown here, show no difference in the rotational envelope in the fluorescence from the linear or T-shaped Ar–I_2 as compared to that of the monomer I_2. Some rotational relaxation is evident in the spectra of all three, which is attributed to collisions within the high-pressure jet; an average of two collisions would make an average loss of four rotational quanta. Second, the peak envelopes are not broadened with decreasing vibrational level in the dispersed fluorescence spectra. This demonstrates that the excess energy is partitioned into translational energy, not rotational excitation. Third, the peak positions (frequencies) are as predicted for a fluorescing I_2 rotational population at low-J levels. The peak positions also do not show a frequency shift which changes with decreasing vibrational level in the dispersed fluorescence spectra. These results are consistent with little to no rotational excitation of the photodissociated I_2, which is as expected if the Ar–I_2 dissociates from either an exactly linear or exactly T-shaped geometry.

Each isomer of Ar–I_2 yields a photofragment distribution that is distinctive in the resultant I_2 fluorescence. In general, the product vibrational distribution of the T-shaped isomer shows a Poisson distribution, with onset of the I_2 product vibrational state (v') appearing at $v'=(v_{\text{pump}}-3)$ for these excitation frequencies. Our results for the T-shaped fluorescence are in excellent agreement with earlier work of Levy and co-workers;[3,4] our data show no improvement upon the earlier fluorescence data of Levy and co-workers, and are not shown.

The dispersed fluorescence spectra of the linear isomer, an example of which is shown in Fig. 2(c), demonstrate how dramatically the vibrational populations of the resulting free I_2 are affected by the transfer of energy from the I_2 oscillator to translational energy of Ar–I_2. This energy transfer is also a dramatic function of the excitation energy. For the highest vibrational excitation ($v_{\text{pump}}=26$), the I_2 transfers an average of about 22% of the I_2 vibrational excitation into kinetic energy of the Ar, and the resultant vibrational distributions are broad and Gaussian. The vibrational distribution is similar to those observed by Valentini and Cross,[7] and by Philippoz *et al.*,[8] for excitations above the I_2 B-state dissociation limit. Our data, taken for excitation energies where the two isomers are distinguishable, clearly show that the abundant linear isomer of Ar–I_2 is responsible for the ''one-atom cage effect'' observed at excitation energies above the B-state dissociation limit.

For lower vibrational excitations ($v_{\text{pump}}=16,18$), the I_2 transfers much less of the vibrational energy into kinetic energy of the Ar, with the distribution for $v_{\text{pump}}=16$ being nearly identical to that observed for the T-shaped isomer, as shown in Fig. 4. Both isomers show strikingly similar vibrational distributions, but different onsets for the I_2 fragment vibrational product states (v'), with $v'=(v_{\text{pump}}-3)$ for the T-shaped isomer and $v'=(v_{\text{pump}}-2)$ for the linear isomer.

For both the T-shaped and linear Ar–I_2 complexes, the onset of the I_2 fragment vibrational product state (v') resulting from the dissociation of the complex reveals information

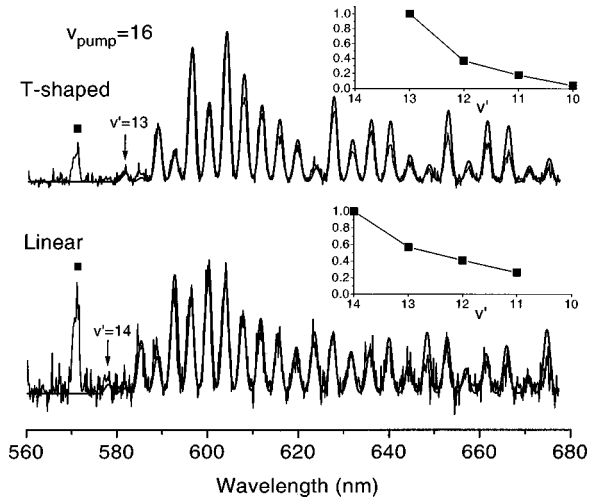

FIG. 4. Dispersed fluorescence spectrum of (a) T-shaped (b) linear Ar–I_2 isomers upon I_2 $B(v_{\text{pump}}=16)\leftarrow X(v'=0)$ excitation. The peaks indicated by ■ are due to laser scattering. The inset diagrams represent the I_2 (B) vibrational product state distributions. Both isomers show strikingly similar Poisson distributions but different onsets of the I_2 product vibrational states (v'), with $v'=14$ for the linear Ar–I_2 and that of $v'=13$ for the T-shaped isomer. The overlapped simulated spectra show excellent agreement with the experiment. The linewidth used in the simulation is 1.65 nm, which is mainly limited by the resolution (300 groves/mm) of the monochromator (as is evident from the laser scattering peak width). Here and in Fig. 6 only the highest frequency feature is labeled. As discussed in the text the more intense lower frequency features are blends of several overlapping bands.

about the ground state binding energy; these energy relationships are shown schematically in the energy level diagram of Fig. 5. As can be seen from the energy cycle of Fig. 5, the photon energy initially deposited into the complex, $h\nu_i$, is equivalent to the sum of the ground state binding energy and total energy of the fragments resulting from the dissociation of the complex; that is,

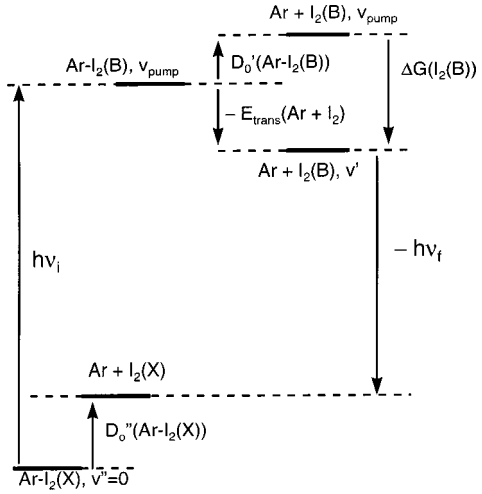

FIG. 5. Energy level diagram showing the relationship between the excitation energy ($h\nu_i$) and fluorescence energy ($h\nu_f$), from which Eqs. (1), (2), and (4) are derived. Note that the energy relationships are correct for *both* the linear and the T-shaped Ar–I_2. Energy increases to the top in the figure, but for clarity the spacing between levels is not proportional to energy. The quantity $\Delta G(I_2(B))$ is defined as the vibrational energy difference between the v' and v_{pump} levels in free I_2, $G(v',I_2(B))-G(v_{\text{pump}},I_2(B))$.

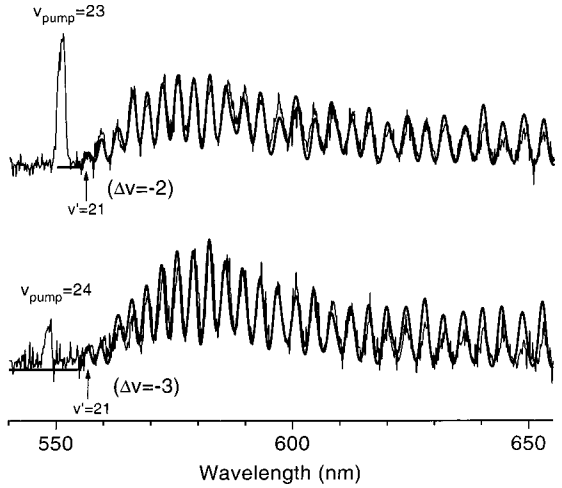

FIG. 6. Dispersed fluorescence spectrum of linear Ar–I_2 following (a) I_2 $B(v_{\text{pump}}=23)\leftarrow X(v''=0)$ excitation at 18 156.4 cm^{-1} and (b) I_2 $B(v_{\text{pump}}=24)\leftarrow X(v''=0)$ excitation at 18 240.2 cm^{-1}, respectively. The peaks labeled by V_{pump} are due to laser scattering. The onset of the I_2 product vibrational state (denoted by arrow) is red-shifted by **two** vibrational quanta with respect to the excitation frequency in (a) and by **three** vibrational quanta in (b). The linear Ar–I_2 ground state binding energy is determined to be $170(1.5)\leqslant D_0(X)\leqslant 174(1.5)$ cm^{-1} (see the text for details).

$$h\nu_i = D_0''(X) + h\nu_f + E_{\text{trans}}(\text{Ar}+\text{I}_2), \tag{1}$$

where $D_0''(X)$ denotes the ground state binding energy of Ar–I_2, $E_{\text{trans}}(\text{Ar}+\text{I}_2)$ is the translational energies of the fragments, and $h\nu_f$ is the final I_2 fragment $B\rightarrow X$ emission photon energy. As noted previously, we have found no evidence of significant product rotational energy (which would be included in $h\nu_f$). The upper limit of Ar–I_2 ground state binding energy, from the limit in which Ar and I_2 separate with zero translational energy, is then given by

$$D_0''(X)\leqslant (h\nu_i - h\nu_f). \tag{2}$$

Equations (1) and (2) are equally valid for either the T-shaped or the linear isomer of Ar–I_2. However, since the $B\leftarrow X$ excitation for the linear isomer is continuous, the photon energy can be varied continuously, and potentially a more accurate limit to $D_0''(X)$ observed; the T-shaped isomer is limited by the discrete band system in the excitation. Figures 6(a) and 6(b) show the dispersed fluorescence spectra of linear Ar–I_2 for excitation to $v_{\text{pump}}=23$ (18 156.4 cm^{-1}) and $v_{\text{pump}}=24$ (18 240.2 cm^{-1}), respectively. We observe the onset of the I_2 product to be $v'=(v_{\text{pump}}-2)=21$ for $v_{\text{pump}}=23$ excitation, which determines an upper limit to $D_0''(X)$ of 174 (± 1.5) cm^{-1}. For $v_{\text{pump}}=24$ excitation, $v'=(v_{\text{pump}}-3)=21$, which is interpreted to mean the $v'=(v_{\text{pump}}-2)=22$ is not accessible because $D_0''(X)$ is greater than the difference in the pump photon energy and the $(B(v'=22)\rightarrow X(v''=0)$ emission energy. A lower limit $D_0''(X)$ of 170 (± 1.5) cm^{-1} is therefore obtained by the energy difference between $v_{\text{pump}}=24$ (18 240.2 cm^{-1}) and I_2 fragment $B(v'=22)\rightarrow X(v''=0)$ emission at 18 069.8 cm^{-1}. The ground state binding energy of linear Ar–I_2 is bracketed to be $170(\pm 1.5)\leqslant D_0''(X)\leqslant 174(\pm 1.5)$ cm^{-1}. All other spectra show vibrational onsets consistent with these limits (but much less accurately bracket the $D_0''(X)$).

If the Ar–I_2 has internal energy, the energetics of the excitation and fluorescence process are such that

$$E_0 + h\nu_i = D_0''(X) + h\nu_f + E_{\text{trans}} + E_{\text{rot}}. \tag{3}$$

The internal energy E_0 consists of rotation and vibration of the Ar–I_2. Some picture of the initial excitation E_0 is obtained under the assumption of thermal equilibrium in the jet. The jet temperature of 15 ± 5 K is taken from detailed studies of hydrogen fluoride expansions in argon performed under similar expansion conditions.[29] The degrees of freedom relevant to the present are most likely internal vibrations, since it is unlikely that rotational energy of the complex may be facilely converted into vibrational energy of *B*-state I_2. The high-frequency vibration of the Ar–I_2 complex is essentially that of I_2, namely, 214 cm^{-1}. At 15 K the population of the first excited state is negligible. The vibrational frequencies of the soft intermolecular modes of the two isomeric forms of Ar–I_2 are similar. For the linear isomer the vibrational interval calculated using the Kunz, Burghardt, and Hess[18] potential is 22.2 cm^{-1} for the degenerate bend. At the nominal jet temperature of 15 K this results in 18% population in this level. The stretching vibrational interval is calculated to be 27 cm^{-1}, resulting in a population of 6% in this level. Adding these two excited populations gives a total excited state population of nearly 25%.

Evaluating the contribution of these excited states, in particular the degenerate bending level, to the estimated dissociation energy is slightly complicated. We first combine the two states and assume that the photofragment distribution is similar to that of the ground state. The vibrational distribution of photofragment *B*-state I_2 following excitation of the higher v_{pump} levels, $v_{\text{pump}}\geqslant 22$ shows a Gaussian distribution, thus the highest v' level produced could result from transitions from excited vibrational levels of Ar–$I_2(X)$. The consequence of this would be to increase our estimate of the dissociation energy by 22.2 cm^{-1}. We do not believe, however, that this occurs. For the excitation of low v_{pump} levels, in particular, $v_{\text{pump}}=16$, the photofragment I_2 vibrational distribution is peaked at the highest v_h' level ($v_h'=14$). This high abundance rules out the production of this level from transitions where the Ar–$I_2(X)$ is excited to the state with one bending quantum. Explicitly, the laser pumping is at 17 516.5 cm^{-1} and the highest energy fluorescence is observed at 17 315.7 cm^{-1}, setting an upper limit of 201 cm^{-1} for the dissociation energy of the complex, D_0''. We make similar arguments for pumping at $v_{\text{pump}}=22$ and probably $v_{\text{pump}}=24$ since here the highest level produced, v_h', has a relative population of 14% and 10%, respectively. If all of the highest level were produced from hot band excitation this requires a quite peaked vibrational distribution in the resulting photofragment I_2. This would mean that the dissociation of the hot bending state is entirely different than the ground state. Physically it is not obvious that the energy in the bending mode will appear in the vibration of the I_2 photofragment. We therefore believe that the error estimate of D_0'' should not be significantly increased from that obtained ignoring the thermal population of the Ar–I_2.

IV. DISCUSSION

In order to carry out a meaningful discussion of the Ar–$I_2(B)$ photodissociation dynamics, we need to establish what is known about the potential curves, i.e., dissociation energies and bond lengths, for the T-shaped and linear isomers in both the X and B states. We take as the starting point our accurate determination of the bond strength for the linear isomer, $170(\pm 1.5) \leqslant D_0''(\text{linear Ar–I}_2(X)) \leqslant 174\ (\pm 1.5)\ \text{cm}^{-1}$. The fact that the linear and T-shaped isomers are both observed in the jet under identical conditions shows directly that the bond energies for the linear and T-shaped isomers must be similar, under the assumption of isomerization equilibrium. Burke[5] has previously estimated that isomeric composition of the jet is $N^{\text{linear}}/N^T = 3$. We note that this estimate was based upon a flat excitation profile for the linear isomer. Here we have found a variation of a factor of two in the excitation profile. This produces an uncertainty in the estimate of the relative absorption of the two isomeric forms. The jet temperature is estimated to be $T = 15 \pm 5$ K. The geometry of the two isomeric forms is known well enough to obtain the ratio of rotational partition functions; at 15 K the rotational partition function of the T-shaped isomer is approximately eight times greater than that of the linear isomer. The contribution of vibration to the partition functions is ignored. Under the assumption of the existence of equilibration between the two forms we calculate that D_0'' of the linear isomer is $(3 \pm 0.5)kT$ larger than that of the T-shaped isomer. This is $30 \pm 12\ \text{cm}^{-1}$, where our error estimate includes a 5K uncertainty in the temperature. We thus calculate that the T-shaped isomer has a bond strength of $142 \pm 15\ \text{cm}^{-1}$. This bond energy can be contrasted with the T-shaped bond energy found by Levy and co-workers of $234.2 \leqslant D_0''(\text{T-shaped Ar–I}_2(X)) \leqslant 240.1\ \text{cm}^{-1}$—a dramatic disagreement. Levy and co-workers used an alternate approach to determine the Ar–I_2 bond energy, which is also evident from Fig. 5. They used the alternate relationship,

$$D_0'(\text{Ar–I}_2(B)) = [G(v_{\text{pump}}, \text{I}_2(B)) - G(v', \text{I}_2(B))] - E_{\text{trans}}(\text{Ar+I}_2), \tag{4}$$

thereby determining the bond energy in the excited B-state Ar–I_2 from the point at which the fluorescence photon energy is largest, which presumably occurs at the threshold where $E_{\text{trans}}(\text{Ar+I}_2)$ equals zero. They then applied the $B \leftarrow X$ blue shift of 14 cm^{-1} to determine the ground-state bond energy. Since our vibrational state distribution for the T-shaped isomer fluorescence is in excellent agreement with theirs, we have no reason to question their fluorescence data. This discrepancy between the expected T-shaped bond energy and the one determined by Levy and co-workers is surprising and unexpected. We conclude that *the highest vibrational level of photofragment* I_2 *produced* following excitation of T-shaped Ar–$I_2(B)$ must be essentially 100% quenched. That is, this level shows nearly 100% ''electronic predissociation'' to the $B''\,{}^1\Pi_{1u}$ state of Ar–I_2, which has a potential curve which is repulsive, i.e., dissociative to I+I and therefore does not fluoresce. Indeed, small intensities at an I_2 vibrational state with $v' = (v_{\text{pump}} = 2)$ are seen in the dispersed fluorescence spectra of Ar–I_2 of Levy and co-workers,[3] which is consistent with those states being energetically accessible, and all but a small fraction quenched. Small intensities in these states are below our poorer signal to noise limit. We therefore conclude that the bond energy in T-shaped Ar–I_2 is weaker by about one quantum of B-state I·I vibration (80 cm^{-1}) than that previously reported. We will return to the dynamical implications of the T-shaped quenching later in this paper.

These bond energies can be compared to the results of the most recent *ab initio* CCSD(T) calculations of Kunz *et al.*, who gave calculated well depths, D_e, of 192.5 cm^{-1} for the linear isomer and 179.2 cm^{-1} for the T-shaped isomer of Ar–I_2. If these are corrected for the zero-point energies, estimated to be about 20 cm^{-1} for the linear isomer and slightly less for the T-shaped isomer, their results give $D_0''(\text{linear Ar–I}_2(X)) \sim 173\ \text{cm}^{-1}$, and $D_0''(\text{T-shaped Ar–I}_2(X)) \sim 160\ \text{cm}^{-1}$. Their calculated energies for the two isomers are thus in close agreement with our determination of the bond energies for the linear and T-shaped isomers in the ground state.

We summarize the known energetics and molecular parameters as follows: The bond energy of the linear isomer is $D_0''(\text{linear Ar–I}_2(X)) = 172(\pm 3.5)\ \text{cm}^{-1}$ (this work); the bond energy in the linear excited state is unknown. The difference in energy between the linear and T-shaped isomers, based on the equilibrium linear to T-shaped ratio of 3:1 (determined from the fluorescence in the jet by Burke[5]) is $D_0''(\text{linear Ar–I}_2(X)) - D_0''(\text{T-shaped Ar–I}_2(X)) = 30 \pm 12\ \text{cm}^{-1}$, from which we estimate $D_0''(\text{T-shaped Ar–I}_2(X)) = 142 \pm 15\ \text{cm}^{-1}$. The blue shift in the $B \leftarrow X$ excitation frequency (determined by Levy and co-workers[4]) $= 13$–$14\ \text{cm}^{-1}$ (depending on vibrational level) dictates that $D_0''(\text{T-shape dAr–I}_2(X)) - D_0'(\text{T-shaped Ar–I}_2(B)) = 14\ \text{cm}^{-1}$, so that $D_0'(\text{T-shaped Ar–I}_2(B)) = 128 \pm 15\ \text{cm}^{-1}$. The rotational contours in the $B \leftarrow X$ fluorescence spectrum were used to estimate the Ar–I_2 bond distances, $R_0''(\text{T-shaped Ar–I}_2(X)) = 4.02$ Å and $R_0'(\text{T-shaped Ar–I}_2(B)) = 4.04$ Å (from Burke[5]). Bond distances in the linear molecule cannot be determined experimentally, because of the continuum excitation spectrum. Finally, we point out that the observation of the distinct fluorescence spectra show that the two isomers of Ar–I_2 are noninterconverting, and the photodissociation dynamics for Ar–$I_2(B)$ occur separately, as seen in this work and the recent work of Burroughs *et al.*[19]

Further discussion of the dynamics of the photodissociation of Ar–$I_2(B)$ is now possible, given the above energetics. We begin with the energy balance equations for the initial preparation of the Ar–$I_2(B)$ state, shown schematically in Fig. 7,

$$h\nu_i = D_0''(\text{Ar–I}_2(X)) + T_0(\text{I}_2(B)) + E_{\text{vib}}(\text{Ar–I}_2(B)) - G(0)(\text{I}_2(B)) - D_e'(\text{Ar–I}_2(B)). \tag{5}$$

In Eq. (5), $h\nu_i$ is the energy of the exciting photon (as in Eq. (1)); $D_0''(\text{Ar–I}_2(X))$ is the bond energy between Ar and $I_2(X)$, or 172 cm^{-1}; $T_0(\text{I}_2(B))$ is the excitation energy of the B state in free I_2, or 15 724.49 cm^{-1}; $E_{\text{vib}}(\text{Ar–I}_2(B))$ is the total vibrational energy in Ar–$I_2(B)$; $G(0)(\text{I}_2(B))$ is the

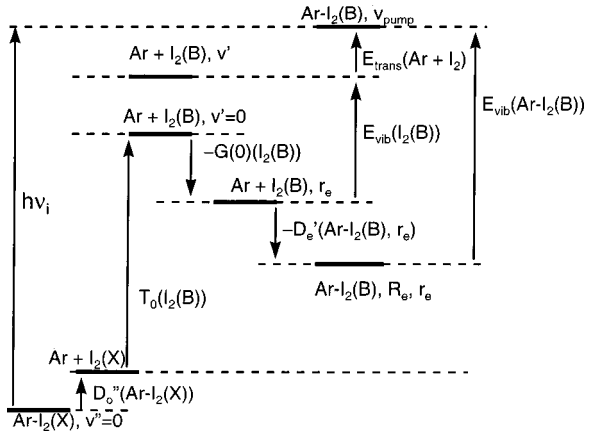

FIG. 7. Energy level diagram showing the total vibrational energy in *B*-state Ar–I_2 as a function of excitation energy, from which Eqs. (5)–(9) are derived. Energy increases to the top in the figure, but for clarity the spacing between levels is not proportional to energy. Note that the vibrational energies $E_{\mathrm{vib}}(\mathrm{Ar–I_2}(B))$ and $E_{\mathrm{vib}}(\mathrm{I_2}(B))$ are defined with respect to zero at the equilibrium bond distances, and the quantity $[E_{\mathrm{vib}}(\mathrm{I_2}(B))+E_{\mathrm{trans}}(\mathrm{Ar+I_2})]$ is defined as the ''available energy,'' E_{avl}, of Eq. (8).

zero point energy of free $I_2(B)$, or 62.54 cm^{-1}; and $D_e'(\mathrm{Ar–I_2}(B))$ is the bond energy between Ar and $I_2(B)$, which is not known. Note that the rotational energy, E_{rot} is assumed negligible, and therefore set equal to zero in Eq. (5), as expected for dissociation of an exactly linear Ar–I_2, and as observed from our spectra and discussed earlier. The vibrational energy in the Ar–I_2 and I–I potentials, with the zero of energy being at the equilibrium bond distances, is found by substitution into Eq. (5),

$$E_{\mathrm{vib}}(\mathrm{Ar–I_2}(B))=h\nu_i-15\,834\ \ \mathrm{cm}^{-1}+D_e'(\mathrm{Ar–I_2}(B)). \tag{6}$$

Following dissociation of the complex, the final vibrational energy in free I_2, $E_{\mathrm{vib}}(\mathrm{I_2}(B))$, which is the observable in this experiment, is given by Fig. 7 and Eq. (7),

$$E_{\mathrm{vib}}(\mathrm{I_2}(B))=E_{\mathrm{vib}}(\mathrm{Ar–I_2}(B))-D_e'(\mathrm{Ar–I_2}(B))-E_{\mathrm{trans}}(\mathrm{Ar+I_2}). \tag{7}$$

The final translational energies of Ar and I_2 are determined by the initial parameters of energy (given by Eq. (5)), bond lengths, and atomic momenta of Ar–$I_2(B)$ (determined from the excitation energy and the Franck–Condon parameters). The trajectories of the Ar–$I_2(B)$ are then determined by the evolution of the excited state on the potential energy surfaces of Ar–$I_2(B)$.

An additional view of the system is to define the available excess energy (energy in excess of the Ar+$I_2(B)$ dissociation limit) of Ar–$I_2(B)$,

$$E_{\mathrm{avl}}=E_{\mathrm{vib}}(\mathrm{I_2}(B))+E_{\mathrm{trans}}(\mathrm{Ar+I_2}), \tag{8}$$

which from substitution of Eqs. (6) and (7), or by examination of Fig. 7, can be seen to be entirely determined by the excitation photon energy,

$$E_{\mathrm{avl}}=E_{\mathrm{vib}}(\mathrm{Ar–I_2}(B))-D_e'(\mathrm{Ar–I_2}(B))=h\nu_i-15\,834\ \ \mathrm{cm}^{-1}. \tag{9}$$

TABLE II. Linear Ar–$I_2(B)$ complex photodissociation energetics.

ν_{pump}	E_{avl} (cm^{-1})[a]	$\langle E_{\mathrm{vib}}\rangle$ (cm^{-1})[b]	$\langle E_{\mathrm{trans}}\rangle$ (cm^{-1})[c]	$\langle E_{\mathrm{trans}}\rangle/E_{\mathrm{avl}}$(%)
26	2568.7	2011.8	556.9	21.7
24	2406.2	1992.4	413.8	17.2
22	2236.1	1975.9	260.3	11.6
20	2058.2	1828.6	229.7	11.2
18	1874.5	1685.6	188.9	10.1
16	1682.5	1553.1	129.4	7.7

[a]E_{avl}, total available energy of photofragments.
[b]$\langle E_{\mathrm{vib}}\rangle$, average vibrational energy of I_2 fragments, obtaining from the product vibrational state distribution data shown in Fig. 3.
[c]Average translational energy of photofragments.

This provides a convenient way to express the partitioning of the excess energy between the resulting vibrational energy of $I_2(B)$ and the recoil translational motion of Ar and $I_2(B)$,

$$\text{average \% recoil translational energy}=100\%\times(E_{\mathrm{avl}}-\langle E_{\mathrm{vib}}(\mathrm{I_2}(B))\rangle)/E_{\mathrm{avl}}. \tag{10}$$

The average $\langle E_{\mathrm{vib}}(\mathrm{I_2}(B))\rangle$ is directly determined experimentally (population fraction in Table I times the $E_{\mathrm{vib}}(\mathrm{I_2}(B))$. The quantities E_{avl}, $\langle E_{\mathrm{vib}}(\mathrm{I_2}(B)\rangle$, and the average percent recoil translational energy are summarized in Table II. A graph of the average percent recoil translation energy is given in Fig. 8. The data points for the $v=16$–26 are from this work; the two points above the *B*-state dissociation energy are calculated by us using the graphical presentation of the vibrational state distributions given by Philippoz *et al.*[8] Figure 8 shows in a very dramatic fashion the substantial difference in vibrational/translational energy distribution on going from the lower v_{pump} excitations to the higher v_{pump} excitations. It also gives a clear presentation that the average percent recoil translational energy reaches a maximum at $\sim v_{\mathrm{pump}}=26$, and further, the average percent recoil translational energy shows no discontinuity between excitation in the bound states versus excitation above the

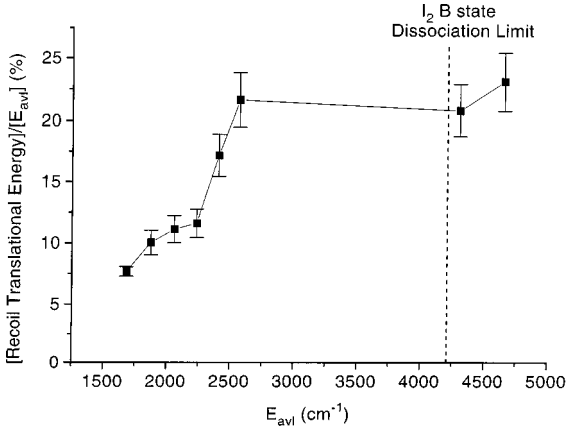

FIG. 8. Average percent recoil translational energy vs total available energy (E_{avl}) graph represents the wavelength dependent photodissociation dynamics of linear Ar–I_2 (B). Data below the I_2 *B* state dissociation limit are taken from Fig. 3 and Table II. Data above the dissociation limit are estimated from Philippoz *et al.* (Fig. 8 in Ref. 8). The percentage of total available energy partitioned into recoil translation shows a sharp increase from $v_{\mathrm{pump}}=16$ (7.7%) to $v_{\mathrm{pump}}=26$ (21.7%) and reaches a plateau (23.2%) above the I_2 *B* state dissociation limit.

B-state dissociation limit. This gives very clear evidence that the caging process observed for excitation to energies above the dissociation threshold has identical molecular dynamics to the process below the dissociation threshold. Stated another way, the process above the dissociation limit therefore does not proceed via a ''dissociation'' followed by a ''recombination'' of the I_2.

We note that Beswick and co-workers[30] proposed a mechanism for the 1-atom cage effect beginning by initial excitation to the repulsive $B''\,^1\Pi_{1u}$ state (perpendicular transition) then undergoing nonadiabatic crossing to the *B* state. This mechanism has been ruled out by Zewail and co-workers.[31]

Quantum dynamical calculations on the photodissociation of $Ar–I_2$ have been reported by several authors, but have only been concerned with the dynamics above the *B*-state dissociation limit.[11,13,14] A relatively detailed treatment is underway by Halberstadt and Janda;[32] their preliminary results do show substantially smaller percent recoil translational energy for the lower v_{pump}. It is beyond the scope of our present work to develop quantum dynamics. We find that a limited development of the classical dynamics of the photodissociation of collinear $Ar–I_2$ provides us insight into the trajectory and the energy transfer from the I–I vibrational coordinate into the Ar translational motion.

The simplest picture of $Ar–I_2(B)$ after excitation is that it consists of a compressed oscillator, the I–I, prepared with zero momentum and with a bond distance equal to the equilibrium distance of the ground state, 2.667 Å. The Ar is considered a ''freely attached particle,'' meaning that the $Ar–I_2$ potential is zero for all distances greater than an arbitrary hard-sphere distance, so that in Eqs. (5) and (6), $D_0'(\text{Ar–I}_2(B))=0$. At the hard-sphere distance the potential (and resultant $Ar–I_2$ force) becomes infinite. The initially prepared $Ar–I_2(B)$ has the Ar to I_2 distance at the hard-sphere value. The Ar is accelerated by the expanding I–I oscillator until it reaches the maximum velocity of the $Ar–I_2$ system, which is at the equilibrium bond distance of *B*-state I_2. At this point, the Ar separates from the I_2, with no further change in its momentum. The $I_2(B)$ oscillator reaches the outer turning point for the reduced vibrational energy. For this classical ball and spring system the final total translational energy is given by

$$E_T=E_{\text{trans}}(\text{Ar}+\text{I}_2)=(M_{\text{Ar}}/(M_{\text{Ar}}+M_{\text{I}_2}))E_{\text{vib}}(\text{Ar–I}_2(B)), \tag{11}$$

in which M_{Ar} and M_{I_2} are the masses of Ar and I_2. This model predicts that the same fraction, 13.6%, of the vibrational energy of $Ar–I_2(B)$ is transferred to translational energy, independent of v_{pump}. The amount of this energy (i.e., number of vibrational quanta lost) will decrease with decreasing $E_{\text{vib}}(\text{Ar–I}_2(B))$. The oversimplification of this most elementary picture may be readily seen from comparison to Fig. 8, in which the average translational energy released as a function of initial excitation is shown; this simple model gives a horizontal line near the average recoil energy.

We chose to model the classical dynamics of $Ar–I_2(B)$ in somewhat more detail by solving Hamilton's equations of motion for the $Ar–I_2$ system prepared with the energy as given by Eq. (5). The $Ar–I_2$ was constrained to linear geometry. We modeled the I_2 potential curve by using a parameterization of the *B*-state RKR potential curve.[33] Three different potentials for $Ar–I_2$ were chosen, namely, a purely repulsive potential modeled by a single exponential,

$$V(\text{Ar–I}_2(B))=A\exp[-\beta(R_{\text{Ar–I}_2}-R_{\text{I}_2})] \tag{12}$$

a simple Morse function,

$$V(\text{Ar–I}_2(B))=D_e\{1-2\exp[-\beta(R_{\text{Ar–I}_2}-R_{\text{I}_2}-R_e)]+\exp[-2\beta(R_{\text{Ar–I}_2}-R_{\text{I}_2}-R_e)]\} \tag{13}$$

and the pairwise diatomics-in-molecules (''DIM'') potential,

$$V(\text{Ar–I}_2(B))=D_e\{2-2\exp[-\beta(R_{\text{Ar–I}_2}-R_{\text{I}_2}-R_e)]+\exp[-2\beta(R_{\text{Ar–I}_2}-R_{\text{I}_2}-R_e)]-2\exp[-\beta(R_{\text{Ar–I}_2}+R_{\text{I}_2}-R_e)]+\exp[-2\beta(R_{\text{Ar–I}_2}+R_{\text{I}_2}-R_e)]\}-Z. \tag{14}$$

The various parameters A, β, D_e, R_e, and Z are taken as adjustable parameters. The bond distance $R_{\text{Ar–I}_2}$ corresponds to the distance between Ar and the center-of-mass of the I_2, and R_{12} is the I–I distance. The form of Eq. (14) is taken from Gray;[34] note that $2D_e$ is the bond energy in the T-shaped isomer of the model potential; the bond energy in the model potential for the linear isomer is somewhat less, and so the zero of energy is adjusted with the parameter *Z*. We chose parameters for the repulsive curve of $A=1–3\times10^8\,\text{cm}^{-1}$ and $\beta=2.4–4.4\,\text{Å}^{-1}$ and parameters for the Morse potential of $D_e=100–200\,\text{cm}^{-1}$, $\beta=2.4–4.4\,\text{Å}^{-1}$, and $R_e=3.82–4.36\,\text{Å}$. For potential of Eq. (14) we used the values $D_e=122\,\text{cm}^{-1}$, $\beta=1.3228\,\text{Å}^{-1}$, and $R_e=4.2003\,\text{Å}$ (all as given by Gray[34]), with $Z=117.9\,\text{cm}^{-1}$.

The purely repulsive potential between Ar and I_2, as in Eq. (12), causes the Ar to be ejected relatively rapidly, with only about 2%–4% recoil translational energy. In effect, the Ar ''does not wait around'' to get a push from the expanding I_2 oscillator. The small vibrational energy transfer seen experimentally in the $v_{\text{pump}}=16$ is somewhat more typical of the purely repulsive $Ar–I_2$ potential. The model shows little change in the percent recoil translational energy as a function of v_{pump}, from $v_{\text{pump}}=16–26$. There are no ''obvious,'' that is, physical realizable, parameters whereby the energy transfer is increased with this pure repulsive model potential.

Either the simple Morse potential, Eq. (13), or the Morse-type potential of Eq. (14) give similar results for the vibrational to translational energy transfer. In the first 0.08 ps, the Ar to I_2 distance decreases, as the I_2 oscillator expands, thereby ''pushing'' the Ar higher on the potential well at the inner turning point of the $Ar–I_2$ potential; this ''push'' is partially responsible for the increased vibrational to translational energy transfer with the Morse-type potentials. The I_2 continues to ''push,'' transferring momentum to the Ar, up to the point at which the I_2 reaches the outer turning point, after ~0.15 ps. The rate of momentum transfer decreases after this, although the Ar continues to accelerate

until about 0.21 ps, when it has reached the distance R_e from the I_2; the Ar slows down slightly after this, as it climbs the potential well to dissociate from the I_2. The Ar slows to 105% of its final velocity after about 0.7 ps, and an Ar–I_2 distance of ~8 Å. For the parameters as given above, we find about 20%–32% recoil translational energy; the 20% value is for $\beta=2.4$ and 32% for $\beta=4.4$. (The percent is not very sensitive to either D_e or R_e.) Although this predicted energy transfer is comparable to the recoil translational energy seen experimentally for higher v_{pump} these models again show no variation in energy transfer as a function of v_{pump}.

In conclusion, our fluorescence data give no direct determination of the potential surface (or even bond energy) of linear *B*-state Ar–I_2. Comparison of our model potentials and classical trajectories to the observed fluorescence suggests: (1) There is no inherent reason for the Ar–I_2 potential to be repulsive to explain the continuum excitation of Ar–I_2. First, the repulsive model potential does not yield final vibrational states which adequately match the observed vibrational distribution in the $I_2(B)$ product. Second, the purely repulsive curve would give a much more rapid, direct photodissociation, such that the fluorescence intensity would show no variation as a function of excitation wavelength, whereas a factor of 2 decrease in the intensity between vibrational bands is observed. Third, a lifetime of Ar–I_2 of 0.15 ps, which is reached at the I–I turning point, corresponds to a lifetime broadening of an individual transition of 18 cm^{-1}. The overall $B \leftarrow X$ band system will therefore be broadened, even if the Ar–I_2 state is bound. The Ar–I_2 ''lifetime'' may be shorter than this; the classical modeling shows that the I_2 has lost about one vibrational quantum of energy (i.e., changed its state) in the first 0.05 ps, corresponding to a lifetime broadening of 53 cm^{-1}. This is remarkably close to the estimate provided by considering a gaussian of full width 57 cm^{-1} centered at each I–I vibrational band, which would result in the observed decrease in intensity between the bands of a factor of 2. We cannot rule out the possibility that the Ar–I_2 is excited onto the repulsive wall of the Ar–I_2 potential, above the Ar–I_2 dissociation limit on the inner turning point, where the energy levels are in the continuum. (2) The vibrational excitations of $v_{\text{pump}}=16-26$ correspond to $r_v(\text{I–I})=3.19$ Å to 3.35 Å (which can be contrasted with $r_e(\text{I–I})=2.667$ Å for $I_2(X)$). The Ar–I_2 interaction potential energy is likely a strong function of the I–I bond distance as well as the Ar–I distance. This has been completely ignored in all quantum calculations on the potential surface, and consequently in the dynamical calculations using those surfaces. Of the above three potentials, only the pairwise potential of Eq. (14) has some dependence on the I–I bond distance—the Ar–I_2 bond energy is about the same, but the Ar–I_2 equilibrium bond length somewhat longer (by 0.18 Å) for longer I–I bond lengths. However, we might surmise that it is somewhat more likely that the Ar–I_2 bonding is weaker for smaller I–I distances (lower v_{pump}), as evidenced by the fact that a dissociative potential more closely mimics the small recoil translational energies for lower v_{pump}, and a bound-state potential more closely mimics the larger recoil energies seen for higher v_{pump}.

Theoretical investigations of Ar–I_2 photodissociation dynamics have been carried out by Martens *et al.* using time-dependent wave packet quantum mechanics and quasiclassical trajectory calculations,[35] based on the Ar–I pair potential obtained from the ZEKE experiments of Neumark and co-workers.[36] Their results, in reasonable agreement with the experiments above *B* state dissociation limit by Philippoz *et al.*,[8] have shown that the final vibrational state distributions of $I_2(B)$ following the photodissociation of the linear Ar–I_2 complex is strongly dependent on the weak Ar–I intermolecular interaction potentials. It is also pointed out by these authors that calculations using an inappropriate Ar–I interaction potential, even based on the collinear Ar–I_2 geometry, shows an I_2 product vibrational state distribution significantly different from the experimental ones. For the photodissociation of the linear Ar–I_2, the final $I_2(B)$ vibrational state distribution directly reflects the initial radial distribution of the complex in the ground electronic state with the reflection mediated by the upper *B* state potential (reflection principle). An unrealistic ground state potential energy surface would not be able to give a true initial radial distribution in the ground state; the electronic excitation of the complex would then vertically propagate the ground-state nuclear wave functions (geometry distributions) onto the *B*-state wave functions. This would make the predicted initial parameters of the *B* state very far from the correct ones, and consequently give rise to incorrect product state distributions. Excited state potential energy surfaces are notoriously inaccurate. Indeed, the dynamical calculations have largely relied on model potentials (e.g., diatomics-in-molecules), which would then cause errors in the Ar–I_2 *B*-state dynamics, amplifying the inaccuracies. It is imperative to obtain high quality ground state and *B*-state potential energy surfaces for Ar–I_2 as a starting point for dynamics occurring in the *B* state. The high rigidity of the ground state, together with the very direct dissociation in the *B* state make it unlikely that large angular excursions can be involved unless the *B*-state potential is very unstable in the linear geometry. Our observation that high rotational levels of I_2 are not populated in the photofragment I_2 lends experimental evidence that such angular excursions play little, if any, role in the photodissociation dynamics. Our work on the linear Ar–I_2, explored much below the I_2 *B*-state dissociation limit, has shown a product vibrational state distribution which is quite a strong function of the excitation energy, which will serve as a stringent test of the accuracy of the Ar–I_2 potential surfaces and dynamical calculations, particularly for the lower excitation energies.

The observation of I_2 $B \rightarrow X$ fluorescence following excitation of the spectrally isolated Ar–I_2 isomers takes place by an initial optical excitation; the excitation is followed by the Ar–I_2 undergoing direct photodissociation, vibrational predissociation, or electronic quenching. The linear Ar–$I_2(B)$ is believed to undergo fast (150 fs), adiabatic ejection of the Ar and suffers no quenching of the *B* state; vibrational predissociation is also not competitive on this time scale.

The dynamics of the T-shaped isomer are extremely complicated; an abbreviated schematic of the processes involved is shown in Fig. 9. The quenching process is broadly

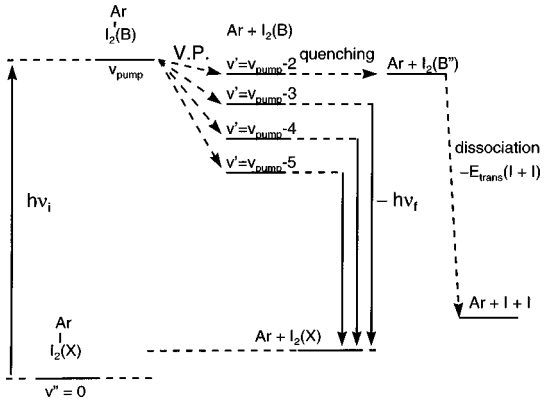

FIG. 9. Energy level diagram showing the dynamical processes for T-shaped Ar–$I_2(B)$. Vibrational predissociation (V.P.) and quenching are both slow, nonadiabatic processes; dissociation of $I_2(B'')$ is a fast, adiabatic process. Note that the state of $Ar+I_2(B)$ for $v'=v_{pump}-2$ is 100% quenched to the B'' state. The excited T-shaped Ar–$I_2(B)$ state prepared at v_{pump} may also undergo vibrational energy transfer to states with the I–I vibrational quantum $v<v_{pump}$, by means of intramolecular vibrational relaxation into Ar–I_2 stretch or bending vibrations, prior to vibrational predissociation (see text).

understood in terms of the interaction of $B\,^3\Pi_{0+u}$ with the repulsive $B''\,^1\Pi_{1u}$. The overall process of excitation of the T-shaped isomer from the ground state to the B state, with subsequent dissociation either into B-state $I_2(v')+Ar$ or into the $B''\,^1\Pi_{1u}$ (which dissociates to $I(^2P_{3/2})+I(^2P_{3/2})+Ar$) may be a complicated admixture of coupled electronic and nuclear motions. As noted by Beswick and co-workers,[9] the $B''\,^1\Pi_{1u}$ is optically connected to the ground state, albeit with lower oscillator strength than the $B-X$ system. Since in I_2 the polarizations of the $B-X$ and $B''-X$ transitions are perpendicular to one another, the excitation spectrum of Ar–I_2 to the $B\,^3\Pi_{0^+u}$ state is probably not mixed coherently with the $B''\,^1\Pi_{1u}$.

Assuming that the T-shaped Ar–$I_2(B)$ has been prepared, vibrational predissociation is observed to be on the same time scale, and therefore competitive with the quenching of the B state.[5] These two processes are conventionally treated as *independent* channels. We suggest the highest energetically accessible vibrational level of B-state I_2 produced in excitation of T-shaped Ar–I_2, is nearly 100% quenched by the Ar. The vibrational predissociation (V.P.) and quenching are shown in Fig. 9. This hypothesis is necessary to account for the discord between the T-shaped bond energies determined from the onset of the vibrational fluorescence (of Levy and co-workers[3,4]) as compared to that estimated in this work by comparison to the linear bond energy. This implies that only states in which the I–I bond stretching vibrational energy has been reduced by at least one quantum can the vibrational predissociation to $I_2(B)(v')+Ar$ be competitive with electronic quenching. This further implies that the vibrational predissociation and electronic quenching channels cannot be treated as independent channels.

Since the vibrational predissociation of T-shaped Ar–$I_2(B)$ is slow, on the time scale of 70 ps (170 I_2 vibrations) it has been argued that an intermolecular vibrational redistribution picture is applicable, in which energy leaks out of the hard I_2 valence oscillation sequentially into the set of soft mode states.[37] A rough picture of the soft mode states is known. The T-shaped isomer has C_{2v} symmetry. The molecule has three vibrational modes, consisting of the stretching of the I–I bond, which is perpendicular to the C_2 axis and of a_1 symmetry; the symmetric stretch of the Ar–I_2, which is parallel to the C_2 axis and of a_1 symmetry; and the angle bending of the Ar–I_2 bond, which is perpendicular to the C_2 axis and of b_1 symmetry. The weak Ar–I_2 stretching frequency is approximately twice the angle bending frequency. Two frequencies 30 and 24 cm^{-1} have been observed;[4] their specific assignment to $\nu_{stretch}$ and $2\nu_{bend}$ is uncertain. We may speculate upon which of the two soft mode motions are effective for electronic quenching and which for the vibrational predissociation. The inner wall of the $B''\,^1\Pi_{1u}$ potential curve lies close to the inner wall of the $B\,^3\Pi_{0^+u}$ state. The symmetry of the $B\,^3\Pi_{0^+u}$ and the $B''\,^1\Pi_{1u}$ states is such that a perpendicular orientation of the perturber (Ar), as occurs in the T-shaped geometry, is required to effect the Ar-induced transition from the fluorescing $B\,^3\Pi_{0^+u}$ to the repulsive $B''\,^1\Pi_{1u}$. This occurs at the *inner* turning point of I_2 and is favored by a short Ar–I_2 distance. Thus the electronic quenching should be selected by the soft modes involving the a_1 Ar–I_2 stretching motion and the a_1 I–I stretch. The vibrational relaxation proceeds through the anharmonic mixing of the a_1 I–I stretch with even quanta of the b_1 bend. Since the bend and I–I stretch are both perpendicular to the C_2 axis, it would appear reasonable to expect them to be coupled. The vibrational predissociation likely depends upon cross terms in the interaction potential between the I_2 valence coordinate and the Ar–I_2 coordinates. Probably these terms are quite anisotropic and therefore can be favored by excitation of the bending motion. The highest free $I_2(B)$ vibrational level produced will have the least translational energy. It will have the slowest rate of separation of the Ar from the I_2, and therefore a longer period of time for the Ar to quench the $I_2(B)$ which has just been created by vibrational predissociation. Thus, we can create a plausible (or consistent) scenario for the observation of near 100% quenching of the highest vibrational state of the nascent $I_2(B)$.

Perhaps even more than for the dynamics of the linear Ar–I_2, there is very little reason to accept the potentials used for calculations of the predissociation. For example, it has been pointed out by Kunz *et al.*[18] that the diatomics-in-molecules potential for the X state of Ar–I_2 does not even show the existence of the two potential minima. The adequacy of the diatomics-in-molecules potential for the B state therefore cannot be regarded as seriously established. In the event that the dynamics are highly coupled to the vibrational modes, it is interesting to point out that no calculations of the Ar–I_2 potential surface have been done in which the I–I bond is allowed to vary. We are aware of only one case, the early calculation by Brown *et al.*[12] on He–I_2, in which the I–I bond distance was varied.

Finally, the role of weak interactions in altering photodynamics is far from obvious. In the broadest view, two diametrically opposite behaviors may be reasonably predicted. The first states that since the interaction is weak, there can be little coupling to the photoexcited chromophore and there-

fore little effect on the dynamics. The second possibility is that all processes essentially proceed through an energy-sharing complex, in which the weakest bond breaks first, thereby producing a substantial change in the dynamical path. It appears that Ar–I_2 follows both extremes. The predissociation time for the T-shaped Ar–$I_2(B)$ is $\sim 10^{-9}$ s, which is three orders of magnitude longer that the dissociation time of $I_2(B)$. The T-shaped isomer, if excited above the *B*-state dissociation limit, therefore proceeds along the I_2 dissociation pathway, with little effect from the Ar atom, i.e., T-shaped Ar–$I_2(B)$ follows the first choice of little effect from the weak interaction. The linear isomer exhibits weak potential coupling; it has essentially the same bond energy as the T-shaped isomer. In this case, the kinetic coupling is maximal, leading to the second type of dynamical behavior in which the Ar so dramatically influences the path that the $I_2(B)$ does not fragment into I+I. The one atom produces a complete cage. The difference in isomeric behavior is essentially geometric, since the coupling is kinetic. It would appear that this is likely to be general since the potential coupling is by definition weak.

We point out that the long-standing puzzle of the origin of the one-atom cage effect in Ar–I_2 is in large measure a consequence of extreme difficulties in predicting the nuclear dynamics of excited electronic states of polyatomic molecules. It is indeed the nuclear dynamics of the T-shaped *B* state isomer which, in our opinion, presents the greatest theoretical challenge; the complete dynamics of excitation and dissociation appears to be an extremely difficult problem involving curve hopping as well as vibrational predissociation.

We return briefly to the question of isomeric forms for the Ne–I_2, Kr–I_2, and Xe–I_2 complexes, for which we did not conduct experiments. Fluorescence from the continuum excitation has been observed by Burke[5] in the corresponding $B \leftarrow X$ region of Kr–I_2. Philippoz *et al.*[8] observed the fluorescence from the high energy excitation of Ne–I_2, Kr–I_2, and Xe–I_2. We attribute this fluorescence to the linear isomers of Ne–I_2, Kr–I_2, and Xe–I_2. The fluorescence data show an increase in energy transfer with increasing mass of the rare gas binding partner. The observed changes, however, are somewhat less than predicted from the extremely simple classical ball-and-spring model of Eq. (11), which depends essentially only upon mass and ignores the variation of Rg–I_2 interaction potential. We made no attempt to model the other Rg–I_2 dynamics with classical models similar to Eqs. (12)–(14).

The complexes with krypton and xenon show no structured fluorescence excitation spectrum from a T-shaped isomer. The lack of observation of T-shaped isomers of the heavier rare gases with I_2 can originate from several different effects, the most likely of these is the electronic quenching of the I_2 *B* state.[38] As has been noted in a collisional quenching study of $I_2(B)$, heavier rare gases are more effective collisional quenchers.[39]

V. CONCLUSIONS

We have used the dispersed intracavity laser induced fluorescence technique to obtain the $I_2(B)$ vibrational product state distribution of linear and T-shaped Ar–I_2 following $B \leftarrow X$ excitation of the complexes. The coexistence of both the linear and the T-shaped isomers of Ar–I_2 under identical conditions is now conclusively established.

Each isomer of Ar–I_2 is distinctive both in the excitation spectrum and the resultant I_2 fluorescence. The T-shaped isomer has well-resolved excitation transitions, and the I_2 fluorescence is sharply peaked at the next highest vibrational level accessible within the energetic constraints of the Ar–I_2 bond dissociation. Our experimental results for the T-shaped fluorescence are in excellent agreement with earlier work of Levy and co-workers.[3,4] The linear isomer has a continuum excitation, and the vibrational populations of the resulting free I_2 are affected by the loss of the Ar. For the highest vibrational excitation ($v_{\text{pump}}=26$), the I_2 transfers an average of about 22% of the I_2 vibrational excitation into kinetic energy of the Ar+I_2. The product $I_2(B)$ vibrational state distribution is similar to those observed by Valentini and Cross,[7] and by Philippoz *et al.*[8] for excitations above the I_2 *B*-state dissociation limit. Our data clearly show that the linear isomer of Ar–I_2 is responsible for the ''one-atom cage effect.'' For lower vibrational excitations ($v_{\text{pump}}=16,18$), the I_2 transfers much less of the vibrational energy into kinetic energy of the Ar+I_2.

Our classical modeling of the Ar–I_2 dynamics of the linear system shows that the linear Ar–$I_2(B)$ lives a fraction of an I_2 vibrational period, with most of the momentum transfer occurring by the time the I_2 has reached the outer turning point of the vibration. The lifetime of linear Ar–$I_2(B)$ of less than 0.15 ps can be contrasted to the 70 ps predissociation lifetime[5,26] of T-shaped Ar–$I_2(B)$.

The origin of the continuum absorption of linear Ar–I_2 is not completely determined by this study. We interpret the data, and our classical dynamics calculations, to suggest that all excitation lines are lifetime broadened so that the resulting band appears as a continuum. The continuum structure may be due to a large bond length increase in Ar–$I_2(B)$ from that in Ar–$I_2(X)$, so that the Franck–Condon allowed transitions are to the repulsive wall at the inner turning point of the potential curve, above the Ar–$I_2(B)$ dissociation limit.

The analysis of the excitation and fluorescent photon energy puts tight limits on the Ar–$I_2(X)$ bond energy; we find this limit to be $170(1.5)\,\text{cm}^{-1} \leqslant D_0''$ (linear Ar–$I_2(X)$) $\leqslant 174(1.5)\,\text{cm}^{-1}$. Relative populations of the linear and T-shaped Ar–I_2 in the jet lead us to conclude that $D_0''(\text{T-shaped Ar–I}_2(X)) \cong 142 \pm 15\,\text{cm}^{-1}$. This can be contrasted to the T-shaped bond energy found by Levy and coworkers, $234\,\text{cm}^{-1} \leqslant D_0'' \leqslant 240\,\text{cm}^{-1}$. We conclude that in T-shaped Ar–$I_2(B)$ fluorescence quenching is most likely an integral part of the dynamics producing vibrational predissociation. Our hypothesis to explain the apparent discord in isomerization energy of Ar–$I_2(X)$ is a strong channel competition in the T-shaped Ar–$I_2(B)$, in which the highest vibrational level of $I_2(B)$ that could energetically be produced from the photodissociation must be essentially 100% quenched by the Ar.

We would greatly enjoy theoretical support for this interpretation. This dramatic, new interpretation of the well-established fluorescence data raises the concern for systems where the fluorescence yield is less than unity that reliable

thermodynamic and dynamical information may not be as directly evident from the fluorescence spectra as has been previously assumed.

ACKNOWLEDGMENTS

We thank Professor K. C. Janda, and Dr. M. L. Burke for helpful discussions, and Dr. D. D. Nelson, Jr. for his assistance in using the SpectraPro-500 Spectrometer. Courteous loan of the SpectraPro-500 Spectrometer from Aerodyne Research is gratefully acknowledged. We thank Professor R. W. Field for his extremely generous loan of the ring dye laser used for these studies. The authors also thank Professor R. J. LeRoy of the University of Waterloo for use of his LEVEL and RKR computer programs. A.E.S.M. thanks the Bunting Institute of Radcliffe College for an ONR Science Scholarship (1996–1998). H.C.F. thanks the Harvard College Research Program for support. This research was supported by the National Science Foundation.

[1] (a) K. C. Janda and C. Bieler, in *Atomic and Molecular Clusters*, edited by E. R. Bernstein (Elsevier, Amsterdam, 1990), p. 455; (b) *Structure and Dynamics of Weakly Bound Molecular Complexes*, Vol. 212 in NATO ASI series, edited by A. Weber (Reidel, Dordrecht, 1987).
[2] G. Kubiak, P. S. H. Fitch, L. Wharton, and D. H. Levy, J. Chem. Phys. **68**, 4477 (1978).
[3] J. A. Blazy, B. M. DeKoven, T. D. Russell, and D. H. Levy, J. Chem. Phys. **72**, 2439 (1980).
[4] K. E. Johnson, W. Sharfin, and D. H. Levy, J. Chem. Phys. **74**, 163 (1981).
[5] M. L. Burke and W. Klemperer, J. Chem. Phys. **98**, 1797 (1993).
[6] K. L. Saenger, G. M. McClelland, and D. R. Herschbach, J. Phys. Chem. **85**, 3333 (1981).
[7] J. J. Valentini and J. B. Cross, J. Chem. Phys. **77**, 572 (1982).
[8] J. M. Philippoz, H. van den Bergh, and R. Monot, J. Phys. Chem. **91**, 2545 (1987).
[9] J. A. Beswick, R. Monot, J. M. Philippoz, and H. van den Bergh, J. Chem. Phys. **86**, 3965 (1987).
[10] I. NoorBatcha, L. M. Raff, and D. L. Thompson, J. Chem. Phys. **81**, 5658 (1984).
[11] M. P. De Miranda, J. A. Beswick, and N. Halberstadt, Chem. Phys. **187**, 185 (1994).
[12] F. B. Brown, D. W. Schwenke, and D. G. Truhlar, Theor. Chim. Acta **68**, 23 (1985).
[13] M. C. R. Cockett, D. A. Beattie, R. J. Donovan, and K. P. Lawley, Chem. Phys. Lett. **259**, 554 (1996).
[14] (a) J.-Y. Fang and C. C. Martens, J. Chem. Phys. **105**, 9072 (1996); (b) A. J. Conley, J.-Y. Fang, and C. C. Martens, Chem. Phys. Lett. **272**, 103 (1997).
[15] S. Zamith, C. Meier, N. Halberstadt, and J. A. Beswick, J. Chem. Phys. **110**, 960 (1999).
[16] F. Y. Naumkin, F. R. W. McCourt, Chem. Phys. Lett. **294**, 71 (1998).
[17] E. Miyoshi, J. Make, T. Noro, and K. Tanaka, J. Mol. Struct.: THEOCHEM **461**, 547 (1999).
[18] C. F. Kunz, I. Burghardt, and B. A. Hess, J. Chem. Phys. **109**, 359 (1998).
[19] A. Burroughs, T. Van Marter, and M. Heaven, American Physical Society Centennial Meeting, Atlanta, GA, March 1999, (Paper No. WC44.89); A. Burroughs, T. Van Marter, and M. C. Heaven, 54th International Symposium on Molecular Spectroscopy, Ohio State University, June 1999 (Paper No. TC11); A. Burroughs, T. Van Marter, and M. Heaven, J. Chem. Phys. **111**, 2478 (1999).
[20] S. J. Harris, S. E. Novick, W. Klemperer, and W. E. Falconer, J. Chem. Phys. **61**, 193 (1974).
[21] K. Higgins, F.-M. Tao, and W. Klemperer, J. Chem. Phys. **109**, 3048 (1998).
[22] X. Xu, W. Jäger, I. Ozier, and M. C. L. Gerry, J. Chem. Phys. **98**, 3726 (1993).
[23] F. Thommen, D. D. Evard, and K. C. Janda, J. Chem. Phys. **82**, 5295 (1985).
[24] D. D. Evard, J. I. Cline, and K. C. Janda, J. Chem. Phys. **84**, 3630 (1986).
[25] D. D. Evard, J. I. Cline, and K. C. Janda, J. Chem. Phys. **88**, 5433 (1988).
[26] J. J. Breen, D. M. Willberg, M. Gutmann, and A. H. Zewail, J. Chem. Phys. **93**, 9180 (1990); D. W. Willberg, M. Gutmann, J. J. Breen, and A. H. Zewail, *ibid.* **96**, 198 (1992).
[27] The I_2 RKR potentials are generated by using the Dunham coefficients taken from S. Gerstenkorn and P. Luc, J. Phys. (Paris) **46**, 867 (1985).
[28] R. J. LeRoy, LEVEL 6.1, A computer program solving radial Schrödinger equation for bound and quasibound levels, and calculating various expectation values and matrix elements, Chemical Physics Research Report, University of Waterloo, October 4, 1996.
[29] H.-C. Chang and W. Klemperer, J. Chem. Phys. **98**, 2497 (1993); C.-C. Chuang, S. N. Tsang, W. Klemperer, and H.-C. Chang, *ibid.* **109**, 484 (1998).
[30] O. Roncero, N. Halberstadt, and J. A. Beswick, Chem. Phys. Lett. **226**, 82 (1994); J. A. Beswick, R. Monot, J. M. Philippoz, and H. van den Bergh, J. Chem. Phys. **86**, 3965 (1987).
[31] C. Wan, M. Gupta, J. S. Baskin, Z. H. Kim, and A. H. Zewail, J. Chem. Phys. **106**, 4353 (1997).
[32] N. Halberstadt and K. C. Janda (personal communication, 1999).
[33] The parameterization is $V(r)=A_j r^j$, with $A_0=6\,763\,318.8$; $A_1=-11\,195\,991$, $A_2=8\,004\,293.2$, $A_3=-3\,233\,812.5$, $A_4=808\,683.77$, $A_5=-128\,298.49$, $A_6=12\,616.465$, $A_7=-703.476\,41$, and $A_8=17.032\,867$, for r in Å and V in cm^{-1}; this form gives convenient derivatives as a function of r. This curve begins to oscillate for I–I distances greater than 5 Å, which does not cause problems because these trajectories never reach those distances.
[34] S. K. Gray, Chem. Phys. Lett. **197**, 86 (1992); Also see S. K. Gray and O. Roncero, J. Phys. Chem. **99**, 2512 (1995).
[35] (a) J.-Y. Fang and C. C. Martens, J. Chem. Phys. **105**, 9072 (1996); (b) A. J. Conley, J.-Y. Fang, and C. C. Martens, Chem. Phys. Lett. **272**, 103 (1997).
[36] Y. Zhao, I. Yourshaw, G. Reiser, C. C. Arnold, and D. M. Neumark, J. Chem. Phys. **101**, 6538 (1994).
[37] E. M. Goldfield and S. K. Gray, J. Chem. Soc., Faraday Trans. **93**, 909 (1997).
[38] M. L. Burke and W. Klemperer, J. Chem. Phys. **98**, 6642 (1993).
[39] J. I. Steinfeld and W. Klemperer, J. Chem. Phys. **42**, 3475 (1965).